Environmental Research 198 (2021) 111295

Contents lists available at ScienceDirect

Environmental Research

journal homepage: www.elsevier.com/locate/envres

Photocatalytic inactivation and destruction of harmful microalgae *Karenia mikimotoi* under visible-light irradiation: Insights into physiological response and toxicity assessment

Wanjun Wang [a,b], Pan Liao [a,b], Guiying Li [a,b], Heng Chen [c], Jingyi Cen [c], Songhui Lu [c], Po Keung Wong [a,b], Taicheng An [a,b,*]

[a] Guangdong Key Laboratory of Environmental Catalysis and Health Risk Control, Guangdong-Hong Kong-Macao Joint Laboratory for Contaminants Exposure and Health, Institute of Environmental Health and Pollution Control, Guangdong University of Technology, Guangzhou, 510006, China
[b] Guangzhou Key Laboratory of Environmental Catalysis and Pollution Control, Key Laboratory of City Cluster Environmental Safety and Green Development, School of Environmental Science and Engineering, Guangdong University of Technology, Guangzhou, 510006, China
[c] Research Center of Harmful Algae and Marine Biology, Jinan University, Guangzhou, 510632, China

ARTICLE INFO

Keywords:
Photocatalysis
Karenia mikimotoi
Marine microalgae
Physiological response
Inactivation mechanism

ABSTRACT

Harmful algal blooms (HABs) caused by *Karenia mikimotoi* have frequently happened in coastal waters worldwide, causing serious damages to marine ecosystems and economic losses. Photocatalysis has potential to *in-situ* inhibit algal growth using sustainable sunlight. However, the inactivation and detoxification mechanisms of microalgae in marine environment have not been systematically investigated. In this work, for the first time, visible-light-driven photocatalytic inactivation of *K. mikimotoi* was attempted using g-C_3N_4/TiO_2 immobilized films as a model photocatalyst. The inactivation efficiency could reach 64% within 60 min, evaluated by real-time *in vivo* chlorophyll-a fluorometric method. The immobilized photocatalyst films also exhibited excellent photo-stability and recyclability. Mechanisms study indicated photo-generated h^+ and $^1O_2$ were the dominant reactive species. Algal cell rupture process was monitored by fluorescent microscope combined with SEM observation, which confirmed the damage of cell membrane followed by the leakage of the intracellular components including the entire cell nucleus. The physiological responses regarding up-regulation of antioxidant enzyme activity (i.e. CAT and SOD), intracellular ROSs level and lipid peroxidation were all observed. Moreover, the intracellular release profile and acute toxicity assessment indicated the toxic *K. mikimotoi* was successfully detoxified, and the released organic matter had no cytotoxicity. This work not only provides a potential new strategy for *in-situ* treatment of *K. mikimotoi* using sunlight at sea environments, but also creates avenue for understanding the inactivation and destruction mechanisms of marine microalgae treated by photocatalysis and the toxicity impacts on the marine environments.

1. Introduction

With the accelerated industrialization and urbanization, harmful algal blooms (HABs) arisen from eutrophication have frequently occurred in coastal marine worldwide (Glibert, 2017; Gobler et al., 2011; Zhang et al., 2019). The HABs occurring in marine are often called red tides, which has posed great threats and damages to marine ecosystems. In addition, some harmful microalgae can secrete toxic substance, which not only aggravates the deaths of fish and shellfish, leading to serious economic losses to aquaculture, but also endangers human health through food chain (Anderson et al., 2012; Lei and Lu, 2011; Paerl et al., 2016).

Among algal species that can form HABs, *Karenia mikimotoi* has received increasing concerns as a rising harmful microalgae that caused HABs over the world (Berdalet et al., 2015; Liu et al., 2020). *K. mikimotoi* was first discovered in Kyoto Bay, Japan in 1935, and then has been successively reported to cause HABs in the coastal marine areas of almost all continents, including Asian, Australia, Europe, South America and North Africa (Landsberg, 2002). The situation has been even worse in China, since the first documented *K. mikimotoi* blooms occurred in

* Corresponding author. Guangzhou Key Laboratory of Environmental Catalysis and Pollution Control, Key Laboratory of City Cluster Environmental Safety and Green Development, School of Environmental Science and Engineering, Guangdong University of Technology, Guangzhou, 510006, China.
E-mail address: antc99@gdut.edu.cn (T. An).

https://doi.org/10.1016/j.envres.2021.111295
Received 16 February 2021; Received in revised form 7 April 2021; Accepted 4 May 2021
Available online 7 May 2021

Hong Kong in 1989 (Yang et al., 2019). One of the most notorious ecological calamities derived from *K. mikimotoi* was reported in the coastal marine areas in Fujian on March 2012. The bloom covered more than 300 km^2 marine areas, which severely damaged the coastal aquaculture, causing countless abalone to die with economic loss of over 2.01 billion (~330 million US dollars) (Li et al., 2017). Recently, *K. mikimotoi* blooms have almost occurred annually in China, with over 100 booms from 2006 to 2019, which is expected to be a longstanding environmental disaster in future. However, current researches on *K. mikimotoi* were focused on the physiology including environmental adaptation, motility, life cycle, as well as toxicity and toxic mechanisms (Li et al., 2019b; Ma et al., 2017), while studies on treatment methods for this species are still rather scare.

Researches on the toxicity behaviors of *K. mikimotoi* to marine organisms has confirmed the lipophilic extracts of this algal cells possess haemolysis and cytotoxicity, but these toxins are merely hypotoxic which cannot induce such high mortality during HABs events (Chang and Gall, 2013). The toxicity effects may be contact-dependent, which suggests that the ichthyotoxicity is caused by the intact algal cell rather than the released toxins (Li et al., 2019b). Therefore, any new treatment methods for control of the *K. mikimotoi* blooms should be able to inactivate and lyse the *K. mikimotoi* cells, so that the toxicity can be compromised. However, current treatment methods for the inactivation of *K. mikimotoi* are limited and mostly based on physical process. For instance, Guan and Li (2017) used UV irradiation to inactivate *K. mikimotoi* with focus on the photoinhibition rate, but the cell structure changes were not studied. Liu et al. (2018) investigated the use of modified clay to remove *K. mikimotoi* by flocculation, and 64% of removal efficiency was reached within 3 h. However, the residual *K. mikimotoi* could grow well to reach a high concentration after the treatment, rising risks for next blooms. In addition, the algal cells might still be intact in the flocs and would transfer to the marine sediments, leading to the persistent toxicity and secondary pollution. Therefore, treatments methods for *K. mikimotoi* with complete destruction of the cell structures are highly desired.

Advanced oxidation processes are well known as green and powerful oxidation technology, in which photocatalysis has been preferred because of its potential to use sustainable solar energy. It has been proven to be able to inactivate a verity of microorganisms, including bacteria, virus, as well as algae. However, current studies about photocatalytic inactivations of algae were mainly focused on freshwater microalgae, such as *Microcystis aeruginosa* (Qi et al., 2020), *Spirulina* and *Anabaena* (Serra et al., 2020), with little attention on the marine microalgae in natural seawater that can form HABs. In this aspect, Lu et al. (2019) used UV-driven photocatalytic system (i.e. UVC/UVA-TiO_2) to inactivate marine microalgae with purpose for ballast water treatment. Natarajan et al. (2018) used TiO_2/Ag/chitosan to treat *Dunaliella salina* under UVC for marine antifouling application. Obviously, the existing few literatures on the topic of photocatalytic inactivation of marine microalgae were mostly based on UV irradiation (Rodriguez-Gonzalez et al., 2010), which could not fully make use of the merits of photocatalysis driven by solar energy. Moreover, the existing photocatalysts were mostly fabricated as powders, which could not be easily recovered if repeatedly used in *in-situ* treatment at sea environments. In addition, although the algal inactivation mechanisms of some freshwater microalgae, typically *Microcystis aeruginosa* have been attempted (Song et al., 2018), the mechanisms for the inactivation of marine microalgae in seawater were not reported.

Herein, photocatalytic inactivation against the typical marine harmful microalgae *K. mikimotoi* in natural seawater was attempted for the first time under visible-light (VL) irradiation. The g-C_3N_4/TiO_2 composites, which has been proven to possess good VL-driven photocatalytic activity to bacterial inactivation (Li et al., 2015; Song et al., 2020) and organic pollutant degradation (Li et al., 2016), were used as the model photocatalysts. The powdery photocatalysts were immobilized on substrates for easy recycling. The *K. mikimotoi* inactivation mechanisms in the light of cell structure changes, major reactive species, antioxidant enzyme activity were analyzed systematically. The release of intracellular organic matter (IOM), the profile of extracellular organic matter (EOM) and the acute toxicity evaluation were all studied. Finally, a tentative VL-driven inactivation mechanism was proposed. The study not only provides a new methodology of using recyclable photocatalyst for the inactivation and detoxification of *K. mikimotoi* in natural seawater, but also provides mechanism insights into the physiological and biochemical stress response of marine microalgae cells towards photocatalysis, especially *in-situ* treatment system at sea environments.

2. Experimental

2.1. Fabrication of immobilized photocatalyst

All the reagents were analytical grade (Aladdin, China) and used without further treatment. The photocatalyst was obtained by fabrication of g-C_3N_4/TiO_2 powders followed by immobilizing on substrates. Briefly, 5 g melamine was placed into an alumina crucible with a lid, which was then annealed at 550 °C for 2 h to obtain g-C_3N_4 powders. Then, different weight percentages of g-C_3N_4 (20, 50, 70 and 90 wt%) and TiO_2 (P25) were mixed in ethanol to prepare a suspension. The suspension was subjected by mechanical stirring for 3 h, followed by ultrasonicating for 1 h at room temperature. The powders of g-C_3N_4/TiO_2 were obtained after drying at 60 °C for 24 h in an oven.

The doctor blade coating technique was used to immobilize g-C_3N_4/TiO_2 powders on substrates (Boonprakob et al., 2014). Generally, 50 mg of the pre-synthesized powder was mixed with 15 μL of acetic acid, 5 μL of Triton X100 and 100 μL of ultrapure water to prepare slurry. Then the slurry was coated on a circular fluorine doped tin oxide (FTO) conductive glass slide (40 × 2.2 mm) with a coating area of 7.065 cm^2. The obtained films on the slides were then heated in static air at 300 °C for 1 h. The obtained samples were characterized with X-ray diffraction (XRD), scanning electron microscope (SEM) and UV–visible diffuse-reflectance spectrum (UV–Vis DRS) techniques (Atinafu et al., 2021). The details can be seen in Supporting Information (SI).

2.2. Photocatalytic inactivation of K. mikimotoi

The *K. mikimotoi* strain used in this work was isolated from Daya Bay, southern China in 2005 (Lei and Lu, 2011). The algae were cultured in sterilized natural seawater with the addition of modified f/2 seawater medium (details of the culture medium was referred in SI) and incubated in a light incubator (MGC-350BP-2, YiHeng, China) at 23±2 °C. The intensity of the incubation was 2000 Lux and the light/dark cycle was 12 h/12 h. The exponential growth period of *K. mikimotoi* was used for the photocatalytic experiments, and the cell density was about 3.78 × 10^4 cells/mL determined by a phytoplankton count box (XKJ-01B, XMDX, China), which was much higher than the cell density in a typical HABs.

A home-made photochemical reactor was applied to evaluate the photocatalytic algal inactivation efficiency. Xenon lamp (PLS-SXE300, PerfectLight, China) with a 420 nm light filter was used as the VL source. The VL intensity was ascertained with a photometer (FZ-A, PerfectLight, China) as 14.2 mW/cm^2. The reaction temperature was kept at 25 °C during the photocatalytic treatment. In a typical experiment, 100 mL K. *mikimotoi* in natural seawater was put in the reactor, followed by adding a piece of the as-prepared g-C_3N_4/TiO_2 coated FTO facing towards the light source. The photocatalytic inactivation experiments were conducted with light irradiation for 1 h. To determine if there was any algal regrowth after the photocatalytic treatment, the treated cell suspension was subjected to a dark adaptation period of 1 h for the algal cells to repair. At given time intervals, 2 mL of the algal cell mixture was taken for analysis. Inactivation efficiency was evaluated by detecting the content of chlorophyll-a by an *in-vivo* chlorophyll fluorometer (FluoroQuik, Amiscience, USA) (Carpentier et al., 2013; Ren et al., 2006), and

calculated by the following Equation (1):

$$\text{Inactivation efficiency}\ (\%) = (1 - C_t/C_0) \times 100 \quad (1)$$

Where C_0 and C_t respectively represents the chlorophyll-a concentration (μg/L) at initial time (0) and any treatment time (t). This method is sensitive and be able to real-time monitor the chlorophyll-a content variation without destroying the cells for extracting the pigments, thus the changes of photosynthetic activity and cell vitality can be *in vivo* and *in situ* investigated during the photocatalytic treatment (Beutler et al., 2002; Harris and Graham, 2015).

2.3. Analytical methods

2.3.1. ROSs analysis

The analysis of $^1O_2$ was studied using FFA (furfuryl alcohol) as the probe (Eugene and Guzman, 2019; Li et al., 2019a), which was determined using HPLC (Agilent 1260–6470, USA) equipped with an Athena C18-WP column (CNW, Germany). NBT (Nitro blue tetrazolium) was used to analyze the produced $\bullet O_2^-$ using UV–Vis spectrophotometer (Cary 100, Agilent) with detecting wavelength of 259 nm (Xia et al., 2015b). Coumarin was used as a trapping agent to monitor •OH production, which was measured by fluorescent luminescence with 332 nm excitation and 460 nm emission (Wang et al., 2019).

2.3.2. Inactivation mechanisms of algal cell

Cell morphological changes of *K. mikimotoi* during the treatment were observed by biomicroscope (B203CED, phenix, China). Different forms of cells including burst cells, round/expanded cells, non-motile cells and swimming cells were counted by a phytoplankton counting box (XKJ-01B, XMDX, China) (Chang, 2011). The variation of cell structure was visually studied through SYTO 9 fluorescence assay, which can stain the nucleus in alive eukaryotic cells, while cannot label cysts or lyse cells (Tawakoli et al., 2013). The cells were stained with SYTO 9 for 15 min in dark, and were observed under a fluorescence microscope (DM6B, Leica Microsystems LTD, Germany). The cell surface morphology changes were studied by SEM (FESEM, SU8220, Hitach, Japan). The morphology change of a single *K. mikimotoi* cell was *in-situ* monitored by a cell imaging multi-mode reader (CYT5MFAV, BioTek, USA). The cell protein was extracted from the cell suspension according to a procedure modified by Fan et al. (2019), and the concentration of proteins was measured by Modified Bradford Protein Assay Kit (C503041, Sangon Biotech). Catalase (CAT) and superoxide dismutase (SOD) activity were determined by CAT Assay Kit (S0051, Boyotime) and WST-8 Kit (S0101, Boyotime), respectively. Intracellular ROSs in algae cells were determined by ROS Assay Kit (S0033, Boyotime) with DCFH-DA as fluorescent probe (Xia et al., 2015a). Malondialdehyde (MDA) concentration as an indicator of lipid peroxidation (Xu et al., 2016) was tested by Lipid Peroxidation MDA Assay Kit (S0131, Boyotime). Details for SEM sample preparation protocol and protein extraction procedure can be found in SI.

2.3.3. Cell release profile and acute toxicity assessment

Organic matter release profile during the inactivation process of *K. mikimotoi* cells was also investigated by TOC analyzer (TOC-L CPH, Shimadzu, Japan) combined with 3D excitation-emission matrix (EEM) fluorescent spectrometer (FS5, Edinburgh, UK). To obtain total organic matter (TOM), the samples containing algal cells lysed with ultrasonic cell pulverizer (JY92-IIN, Xinzhi, China) for 10 min, and then measured after filtered by 0.22 μm membrane (PES, Cool Wind, China), according to the protocol reported by Jin et al. (2019). Extracellular organic matter (EOM) was obtained by directly measuring the filtered samples without cell lysis procedure. Intracellular organic matter (IOM) was then obtained by the differences between TOM and EOM. The release profile of EOM was analyzed by fluorescence EEM spectrometer, and MATLAB was used for data processing (Tian et al., 2018). Inorganic ions release profiles were measured by ICP-MS (ICAP RQ, Thermo Fisher, Germany). At given intervals, 10 mL solution was withdrawn and passed through 0.45 μm membrane (PES, Cool Wind, China). Measurements were conducted after the filtered solution was digested at 140 °C for 15 min with concentrated HNO_3.

Acute toxicity was tested with bioluminescent bacteria *V. fischeri* according to Wang et al. (2017). Both sample solutions with and without algal cells were tested. In a typical test, 2 mL collected sample was blended with 1 mL of *V. fischeri* and adapted for 15 min, which was then tested by intelligent biological toxicity tester (DXY-3, KTY, China). *V. fischeri* incubated in seawater medium was used as control group. Acute toxicity was evaluated by the inhibition ratio (IR) of bioluminescence, which was obtained by the following Equation (2):

$$\text{IR}\ (\%) = (I_c - I_s)/I_c \times 100 \quad (2)$$

where I_c and I_s are the bioluminescence intensity of the control group and sample solutions, respectively.

3. Results and discussion

3.1. Photocatalyst characterization

Crystal structure of the as-synthesized g-C_3N_4/TiO_2 films was examined with XRD. The diffraction peaks at 27.5°, 36.1°, 41.2°, 54.3°, 56.6° and 69.0° can be assigned to (110), (101), (111), (211), (220) and (301) phase of TiO_2 (Fig. S1(a)) according to the references (Chen and Lou, 2010), while the peaks at 27.7° can be indexed as (002) diffraction plane for graphitic structure in g-C_3N_4 according to references (Feng et al., 2018; She et al., 2014). With the increase of g-C_3N_4 ratio in the film composite, the intensity of featured peaks of g-C_3N_4 was enhanced with decreased TiO_2 peak intensity (Fig. S1(b)). Optical properties of as-prepared g-C_3N_4/TiO_2 films were analyzed by UV–vis absorption spectroscopy. As the g-C_3N_4 ratio in the composite film increased, the VL absorption region of g-C_3N_4/TiO_2 was expanded to longer wavelength (Fig. S2). Morphologies of the samples were also investigated by FESEM (Figs. S3(a–c)). The pure g-C_3N_4 showed layered nanosheet structure, consistent with previous reports (Tong et al., 2015), while pure TiO_2 appeared as spherical nanoparticles with sizes of ~300 nm. The g-C_3N_4/TiO_2 composites exhibited spherical nanoparticles embedded layered structure, suggesting the TiO_2 particles were evenly attached to the g-C_3N_4 surface. This was further verified by the EDX spectrum and corresponding element mapping (Figs. S3(d–h)), which showed the elements of C, N, O and Ti were dispersed evenly without other impurities. These results confirmed the successful synthesis of g-C_3N_4/TiO_2 film for the subsequent algal inactivation experiments.

3.2. Inactivation efficiency against K. mikimotoi

As an essential photosynthetic pigment, Chlorophyll-a is present in almost all phytoplankton species including *K. mikimotoi*. It is commonly utilized as an indicator to quantify algal biomass, thus evaluating the status of eutrophication and HABs in coastal waters (Lapointe et al., 2015; Toming et al., 2016). In addition, the chlorophyll-a content is in proportion to the vitality of algal cells, and therefore has been widely used to evaluate the inactivation efficiency during algal inactivation experiments. As shown in Fig. 1(a), the dark control experiments using 50 wt% g-C_3N_4/TiO_2 film without VL irradiation show that the chlorophyll-a content remains almost unchanged, suggesting the photocatalysts alone has negligible inactivation effects to *K. mikimotoi* in dark. It was interesting to find that, with VL irradiation, the chlorophyll-a contents in all treatment systems were decreased dramatically in the initial 10 min and reached a steady value at 60 min of VL irradiation. It seems that the *K. mikimotoi* could be affected under VL irradiation even without photocatalysts. However, when the treated *K. mikimotoi* cells were adapted to a subsequent dark period, the cells in

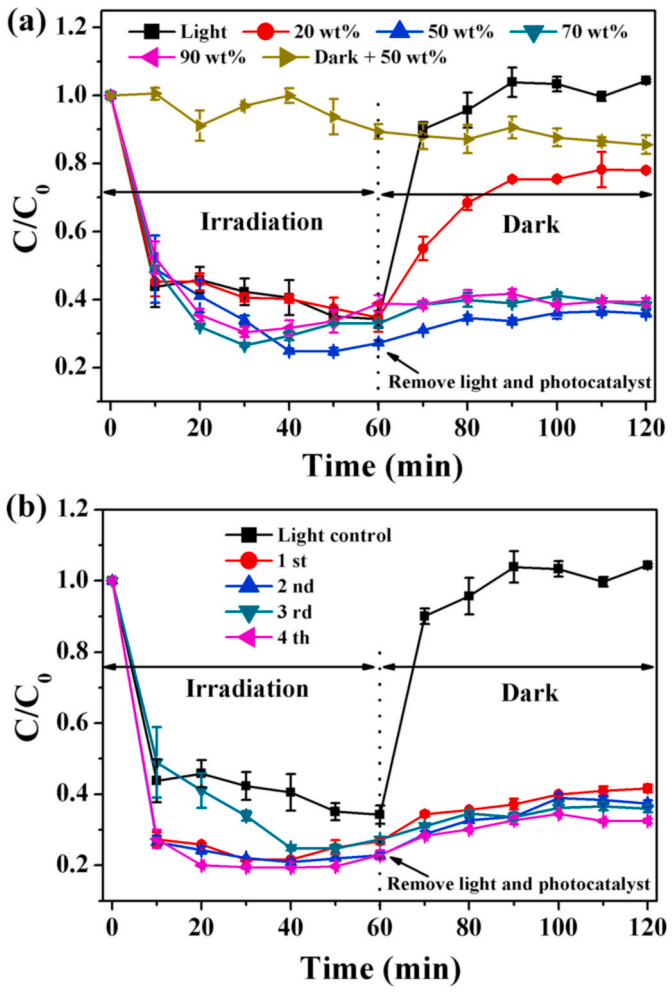

Fig. 1. (a) Photocatalytic inactivation efficiency of *K. mikimotoi* evaluated by *in vivo* Chlorophyll-a fluorescence over g-C_3N_4/TiO_2 films with different g-C_3N_4: TiO_2 ratio of 20–90 wt% g-C_3N_4 under VL irradiation ($\lambda \geq 420$ nm). Dark adaptation was applied after 60 min of treatment; (b) Recycling experiments for photocatalytic inactivation of *K. mikimotoi* with four successive cycles using 50 wt% g-C_3N_4/TiO_2 films as photocatalyst.

the light control group were recovered gradually as the chlorophyll-a returned to the same level of starting point after 60 min dark adaptation. In contrast, the chlorophyll-a fluorescence could not be recovered in the existence of g-C_3N_4/TiO_2 as photocatalysts (Fig. 1(a)). This phenomenon could be ascribed to the fact when light irradiance exceeded the photosynthesis requirements of algal cells, their photosystem II (PSII) reaction center would be closed to protect photosynthetic apparatus from high-light injury (Ruban et al., 2012). When subjected to a subsequent dark condition, the PSII reaction center of algae would re-open and immediately produce chlorophyll-a fluorescence, while the algae with damaged PSII could not produce fluorescence. This suggests that the PSII of *K. mikimotoi* cells were damaged during the photocatalytic inactivation process. Therefore, a dark adaptation period must be applied after the light irradiation, in order to accurately evaluate the damage of photosynthetic system of algal cells. The inactivation efficiency evaluated by inhibition of chlorophyll-a fluorescence after 60 min dark adaptation were obtained to be 22%, 64%, 62% and 61% for 20 wt%, 50 wt%, 70 wt% and 90 wt% g-C_3N_4/TiO_2, respectively. This indicates that the inactivation efficiency was increased with the enhancement of g-C_3N_4 ratio from zero to 50%, and slightly decreased with the g-C_3N_4 ratio further increased to 90%. The highest inactivation efficiency was acquired by 50 wt% g-C_3N_4/TiO_2 film which was used thereafter in this work.

To explore the photo-stability and recyclability, the used 50 wt% g-C_3N_4/TiO_2 film on the glass substrates was easily recovered and put into another set of *K. mikimotoi* seawater suspension, and four successive cycling reactions of *K. mikimotoi* inactivation were conducted. It was found that the immobilized film exhibited stable photocatalytic activity, since a high inactivation efficiency of 67% was still achieved after four cycles of experiments (Fig. 1(b)). The crystal structure of the g-C_3N_4/TiO_2 film did not change after the reactions (Fig. S4), confirming the high photo-stability of the as-prepared films. In addition, no observed particles of photocatalysts were released from the substrates after four cycles, which further confirmed the high adhesion capability and recyclability of the as-prepared photocatalysts, showing good potential for *in-situ* treatment of microalgal at sea water environments.

3.3. Roles of reactive species

To study the inactivation mechanisms of *K. mikimotoi*, two major issues need to be addressed. One is the function of different reactive species in algal cell inactivation. The other is physiological changes during cell inactivation process. The possible generated reactive species during photocatalysis include •OH, $\bullet O_2^-$, $^1O_2$ and H_2O_2. Their roles in the inactivation of *K. mikimotoi* were studied by scavenging study. The scavengers used were Cr (VI) for e^-, sodium oxalate for h^+, furfuryl alcohol (FFA) for $^1O_2$, 4-hydroxy-2,2,6,6-tetramethylpiperidine-1-oxy (TEMPOL) for $\bullet O_2^-$, isopropanol (IPA) for •OH and Fe (II) for H_2O_2 (Wang et al., 2012; Xia et al., 2015b). It was found that the additions of IPA, TEMPOL and Fe(II) had negligible impact on the inhibition efficiency of *K. mikimotoi* (Fig. 2(a)), suggesting •OH, $\bullet O_2^-$ and H_2O_2 were not the dominant reactive species. In contrast, additions of oxalate and Cr(VI) could significantly inhibit the inactivation efficiency, since only 47% and 52% of inactivation was obtained after 60 min treatment, respectively. In addition, FFA was found to obviously suppress the inactivation efficiency, which indicated that $^1O_2$ was also involved in this reaction process. The generation of $^1O_2$ ($k = 1.20 \times 10^8$ M^{-1} s^{-1}) was further quantitatively analyzed by the decline of FFA as a probe (Fig. 2(b)). By evaluating the apparent rate constant of FFA, the steady-state concentration of $^1O_2$ was calculated to be 3.48×10^{-12} M. Moreover, the radical generation was further verified by ESR spectroscopy using TEMP as spin-trapping reagent. As shown in Fig. 2(c), the obvious and gradually amplified signals of TEMP-$^1O_2$ were observed with prolonged reaction time, further confirming the production of $^1O_2$. The production of $^1O_2$ might be originated from $\bullet O_2^-$ by the following reactions (Equations (3) and (4)) according to reference (Mourad et al., 2019):

$$e^- + O_2 \rightarrow \cdot O_2^- \quad (3)$$

$$2 \cdot O_2^- \rightarrow O_2^{2-} + x^3O_2 + (1-x)^1O_2 \quad (4)$$

The above production pathway of $^1O_2$ was further confirmed by quantitatively analysis of $\bullet O_2^-$ using NBT as the probe. The NBT could quickly react with $\bullet O_2^-$ with a rate constant k of 5.88×10^4 M^{-1} s^{-1}. As shown in Fig. 2(d–e), the absorbance of NBT solution (0.025 mM) at 260 nm was decreased under VL excitation. The calculated steady-state concentration of $\bullet O_2^-$ was 2.01×10^{-8} M. However, the addition of TEMPOL had no inhibition effects on the efficiency (Fig. 2(a)), probably due to the fact that only tiny amount of $\bullet O_2^-$ was generated and spontaneously transformed to $^1O_2$. The production of •OH was also studied by using coumarin as the trapping agents, and no peaks corresponding to 7-hydroxylcoumarin were found under VL irradiation (Fig. S5). In addition, the production of H_2O_2 was investigated using DPD method (Moon et al., 2014), and no H_2O_2 was detected (data not shown). These results were consistent with the above scavenging experiment result that $^1O_2$ was more important than •OH or $\bullet O_2^-$ for the inactivation of *K. mikimotoi* in this system, which may be attributed to the significantly high life time of $^1O_2$ ($\tau_{1/2} < 10$ μs) compared with •OH/$\bullet O_2^-$ ($\tau_{1/2} < 1$ ns)

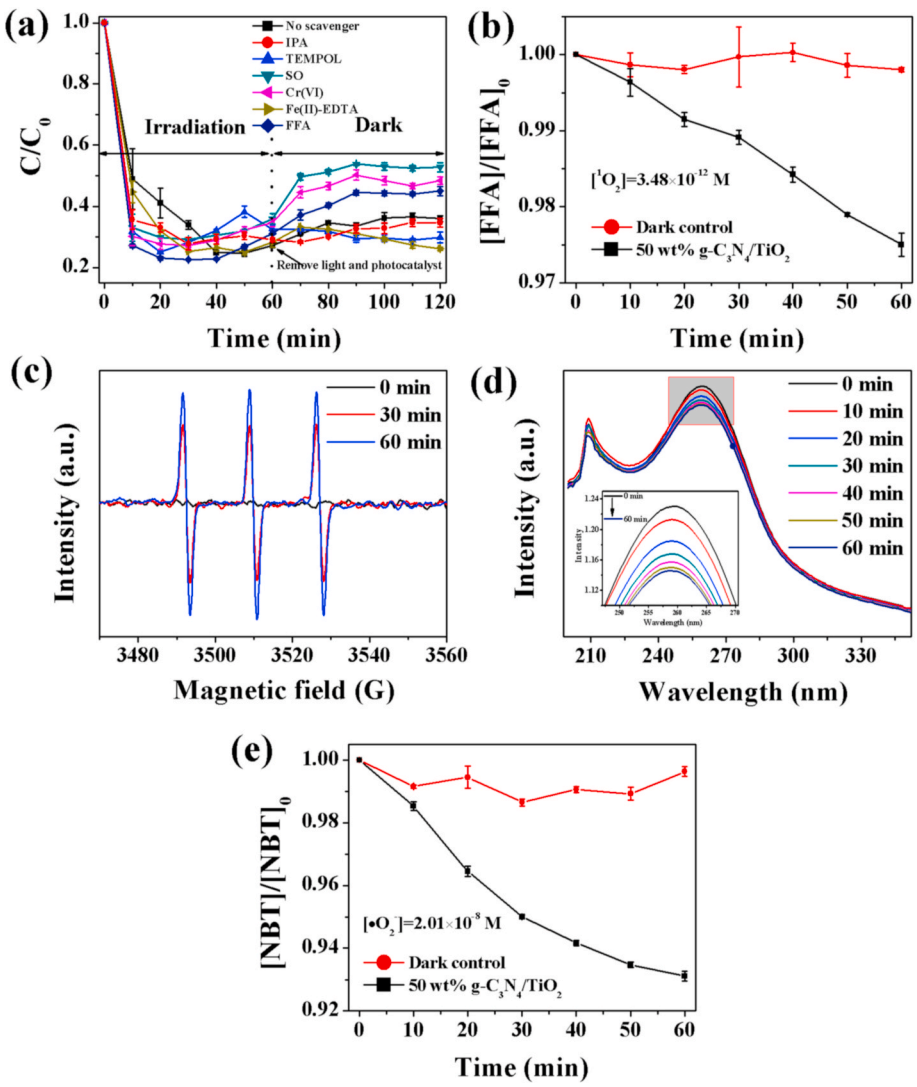

Fig. 2. (a) Photocatalytic inactivation efficiency of *K. mikimotoi* evaluated by *in vivo* Chlorophyll-a fluorescence under VL irradiation ($\lambda \geq 420$ nm) with different scavengers ([oxalate] = 0.5 mM, [Cr(VI)] = 0.05 mM, [IPA] = 0.5 mM, [FFA] = 1 mM, [TEMPOL] = 1 mM, [Fe(II)] = 0.1 mM). Dark adaptation was applied after 60 min of treatment; (b) Time-dependent concentration changes of FFA as $^1O_2$ probe; (c) Electron spin resonance (ESR) spectra of TEMP spin-trapping adducts ($^1O_2$) during the photocatalytic algal inactivation under the VL irradiation ([TEMP] = 1 mM, $\lambda \geq 420$ nm). (d) Changes of absorption spectra of NBT (0.025 mM) as $\bullet O_2^-$ probe; (e) Time-dependent concentration changes of NBT detected at 259 nm.

(You and Nam, 2014). In fact, the photo-generated h^+ are transferred to the valence band (VB) of g-C_3N_4 instead of TiO_2 based on our previous research (Li et al., 2015), and the VB potential ($E_{VB} = 1.65$ V) of g-C_3N_4 is not high enough to generate •OH ($E_{\bullet OH/OH^-} = 1.99$ V) (Fu et al., 2012). Therefore, no •OH was produced in this system. These results confirmed the h^+ and $^1O_2$ were the primary reactive species to inactivate *K. mikimotoi*.

3.4. Inactivation mechanisms of K. mikimotoi

The destruction of cell structure is crucial for *K. mikimotoi* inactivation and detoxification. Thus, the morphological changes of *K. mikimotoi* cells during photocatalytic inactivation process were visually studied through optical microscope combined with fluorescent microscope and SEM observation. At the initial stage, the *K. mikimotoi* cell exhibited a clear oval shape with size of 26.3 μm in width and 33.1 μm in length, which could swim freely in water (Fig. 3(a)). After 10 min of treatment, the cells became round cells, while the green pigments could still be observed (Fig. 3(b)). Then, the cells were further transformed to expanded cells with weaker green pigments (Fig. 3(c)). Finally, burst cells were found with even weaker pigments and ruptured cell membrane (Fig. 3(d)). After staining with SYTO 9, the green fluorescence emitted by nucleus of *K. mikimotoi* cells and the red fluorescence emitted by chloroplast of *K. mikimotoi* cells were observed in Fig. 3(e–g). It was interesting to find the nucleus of *K. mikimotoi* cells disappeared after 50 min of treatment (Fig. 3(h)), which indicated that the cell membrane was severely damaged to form a highly porous structure and even cause the dissolve or leakage of entire cell nucleus. This was further verified by real-time *in-situ* monitoring a single *K. mikimotoi* cell on a cell imaging multi-mode reader, which clearly showed the gradual disappear of nucleus with reaction time (Fig. S6). In addition, the surface morphology change of *K. mikimotoi* cells was also studied by SEM (Fig. 3(i–l)). The untreated *K. mikimotoi* cell was intact at the beginning stage, although the cell envelope exhibited rough due to the dehydration process in SEM sample preparation (Fig. 3(i)). With treatment, the cell surface clearly became porous, and an obvious big pit (marked with red cycle) was found after 30–50 min of treatment (Fig. 3(k)), probably resulted from the leakage of the nucleus, which coincided with the phenomenon in Fig. 3(h). Finally, only cell debris was observed within 50 min of treatment (Fig. 3(l)). Based on the above observation results, it demonstrated that *K. mikimotoi* cells were indeed suffered from severe attacks of ROSs, leading to irreparable damage of cell membrane, leakage of intracellular components, cell rupture and final death. To quantitatively understand the cell rapture process, the numbers of different status of *K. mikimotoi* cells (50 μL, diluted 5 times) were counted by a phytoplankton count box based on optical microscope observation. As shown in Fig. 4, it was found that the proportion of bust cells reached 98% after the photocatalytic treatment for 1 h, which was

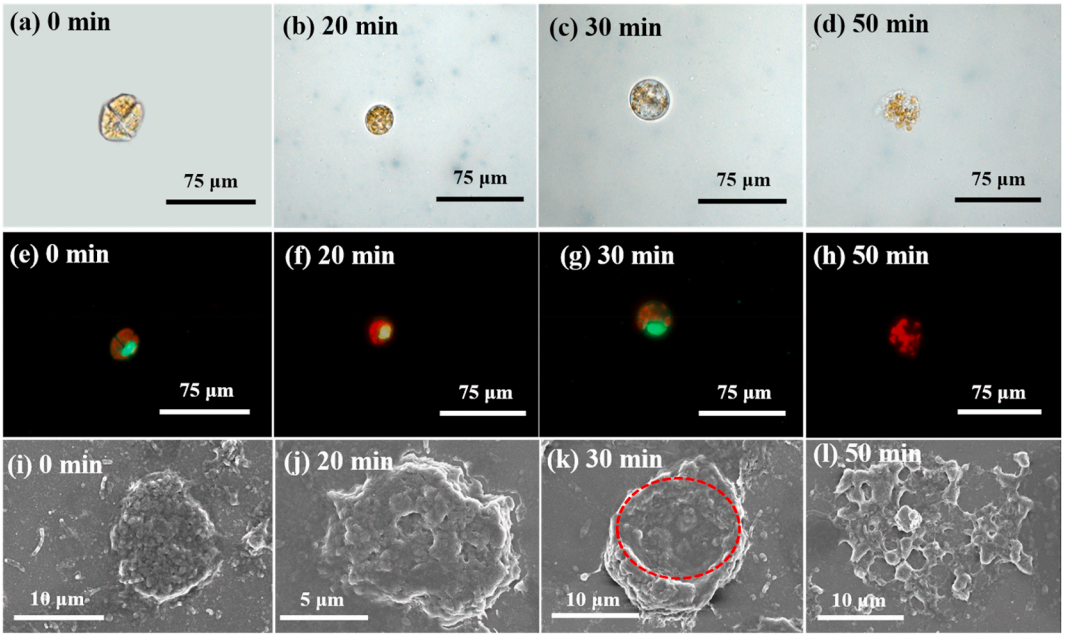

Fig. 3. (a–d) Optical microscopic images, (e–h) corresponding fluorescence microscopic images after staining with SYTO 9 and (i–l) scanning electron microscope (SEM) images of *K. mikimotoi* cells during photocatalytic inactivation under VL irradiation ($\lambda \geq 420$ nm) at different intervals (0 min, 20 min, 30 min and 50 min).

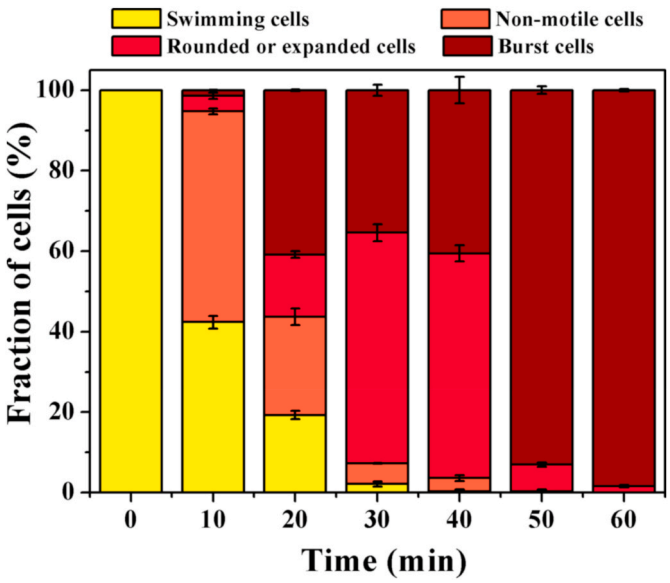

Fig. 4. Variation of swimming, non-motile, rounded/expanded and burst cell fractions during the photocatalytic inactivation of *K. mikimotoi* by g-C_3N_4/TiO_2 film under VL irradiation ($\lambda \geq 420$ nm).

consistent with the inactivation efficiency measured by chlorophyll-a content, and was also much higher than previous reported clay flocculation method for *K. mikimotoi* removal (Liu et al., 2018).

To further understand the inactivation mechanisms, several intracellular physiological characteristics of *K. mikimotoi* were monitored. Total soluble protein is essential in microorganisms and reflects the cell metabolism activity (Zhang et al., 2013). The protein content appeared an increase in the first 5 min of treatment then decreased to an extremely low level after subsequent 55 min of treatment (Fig. 5(a)). This indicated that when subjected to oxidative stress, the *K. mikimotoi* cells promptly synthesized large amounts of soluble protein within initial 5 min, thereby providing more metabolic enzymes to resist the adverse environment. However, when adverse stress exceeded the tolerance limit of the algae, the protein synthesis was impaired, leading to the reduction of protein content. Two important intracellular antioxidant enzymes of catalase (CAT) and superoxide dismutase (SOD) that can protect cells from oxidative damage were studied. SOD can dismutase $\bullet O_2^-$ into H_2O_2, while H_2O_2 can be further decomposed to water and oxygen by CAT (Bhuvaneshwari et al., 2018; He et al., 2012). As shown in Fig. 5(b–c), in the initial 5 min, neither SOD nor CAT was activated, probably due to the increase of soluble protein (Fig. 5(a)). Then, CAT and SOD levels gradually increased with treatment time, indicating that there were large amounts of oxidizing radicals attacking the algal cells, leading to the induction of SOD and CAT to compromise the oxidative stress. To further understand the physiological response, intracellular ROSs level was monitored by DCFH-DA probe according to referred method (Wang et al., 2019). Results show that the intracellular ROSs level was decreased in the first 5 min (Fig. 5(d)), which was ascribed to the up-regulation of protein synthesis. With the protein content began to drop, the intracellular ROSs level began to increase after 5 min treatment, indicating that the algae cells could no longer maintain cell metabolism to resist external stress, thereby antioxidant enzyme defense system was activated to compromise the attack of ROSs.

Malondialdehyde (MDA) is the major product of lipid peroxidation to indicate the oxidative damage of algal cell membranes (Liu et al., 2018). It was found that MDA level increased rapidly in the initial 10 min, and then dropped to a normal level at about 20 min (Fig. 5(e)). This suggests that cell membrane was the first attacking sites which caused the lipid peroxidation and subsequent increase of cell membrane permeability, allowing the entrance of more photo-generated ROSs. Thus, the intracellular antioxidant enzyme system was activated (i.e. up-regulation of CAT and SOD) to quench the ROSs, leading to the rapid decrease of lipid peroxidation after 10 min. It was found that the MDA level was re-raised in the late stage at 30 min, which could be due to the over-accumulation of ROSs inside the cells cause the dysfunction of antioxidant enzyme system and subsequent cell necrosis. On the contrary, no significant changes of SOD, CAT and MDA activity and intracellular ROSs level were observed under dark control experiments. These evidences confirmed the ROSs-induced oxidative physiological response of *K. mikimotoi* under photocatalytic treatment.

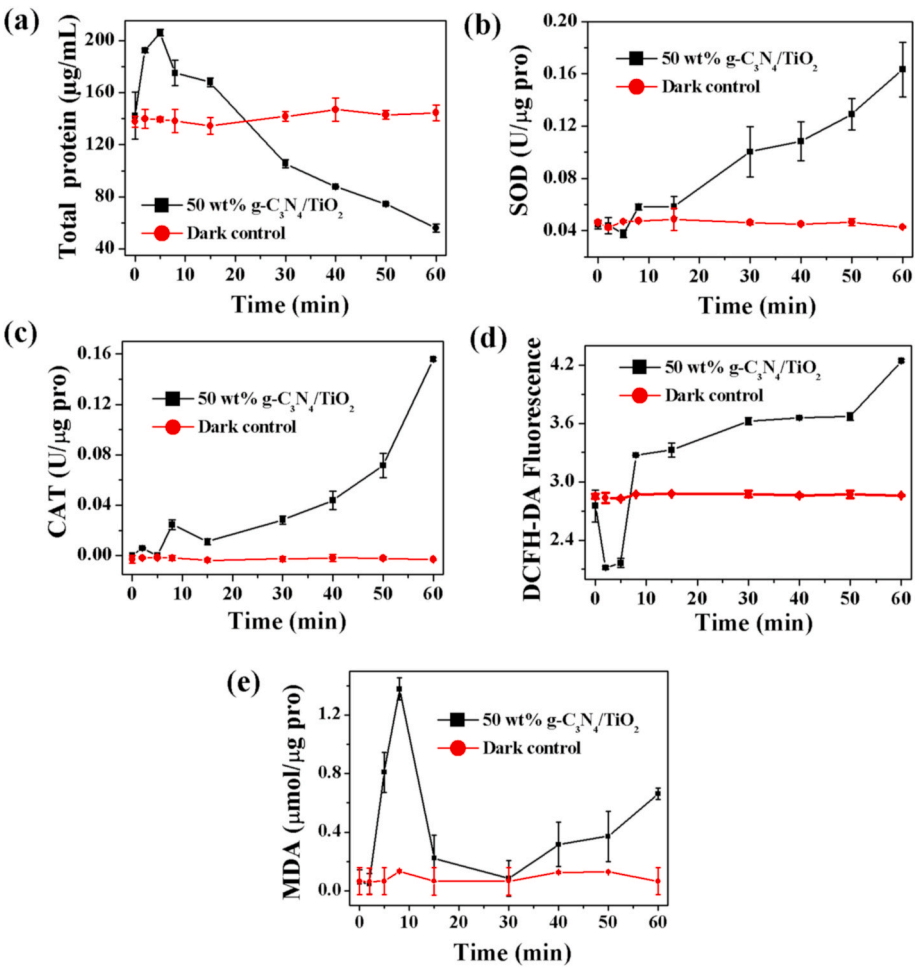

Fig. 5. Changes of (a) total soluble protein content, (b) superoxide dismutase (SOD) activity, (c) catalase (CAT) activity, (d) intracellular ROS level and (e) malondialdehyde (MDA) level during photocatalytic inactivation of *K. mikimotoi* cells under VL irradiation ($\lambda \geq 420$ nm).

3.5. Intracellular release profile and toxicity assessment

To evaluate the impact to the marine environment after the photocatalytic treatments, intracellular release profile and acute toxicity were investigated during photocatalytic inactivation process. The organic matter in this marine microbial system can be classified as IOM and EOM. Fig. 6 depicts that during the inactivation process of *K. mikimotoi*, the IOM was gradually decreased obviously with the increase of EOM, due to the rupture of cell membrane causing the IOM to be released to the environment. It was estimated that 71% of IOM was released from cells after 1 h of photocatalytic treatment, which might cause secondary pollution to the marine environment. Thus, the release profile was further studied by three-dimensional fluorescence EEM (Li et al., 2014; Ou et al., 2011), which can provide additional insights into the composition of released organic matter. Fig. 7 shows the EEM of released organic matter with different reaction time during the inactivation process of *K. mikimotoi*. Two peaks at $\lambda_{ex}/\lambda_{em}$ of 260/520 nm (peak A) and 275/345 nm (peak B) were observed at the initial stage (Fig. 7(a)), which was indexed to humic-like and fulvic acid-like substances, respectively. With 10 min of treatment, a new fluorescent peak at $\lambda_{ex}/\lambda_{em}$ of 240/370 nm (peak C) was observed (Fig. 7(b)), which corresponds to tryptophan-like substance according to previous reports (Murphy et al., 2006, 2011). With prolonged treatment time to 60 min, the fluorescent peaks of A and B were both disappeared, with fluorescent peak C steadily increased (Fig. 7(c–g)), suggesting that humic-like and fulvic acid-like substances were degraded while tryptophan-like substances in cells leaked into seawater during the photocatalytic inactivation process. Tryptophan is considered to be an important amino acid to constitute proteins in aquatic life, which would not cause significant negative impacts to the marine environments (Favero and

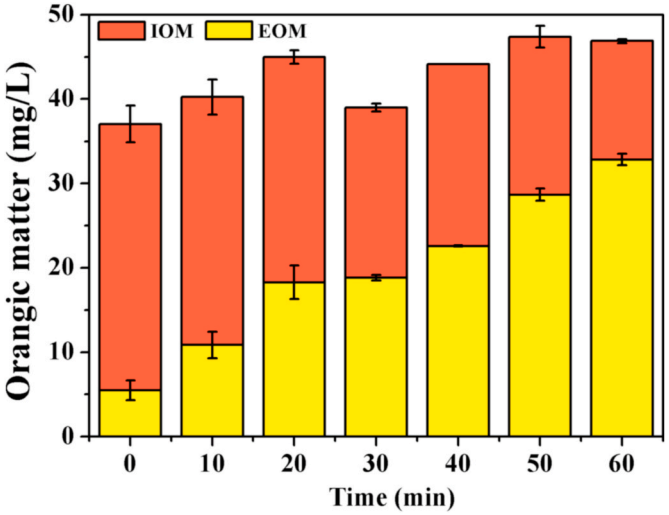

Fig. 6. Temporal profiles of intracellular organic matter (IOM) and extracellular organic matter (EOM) in *K. mikimotoi* cell suspensions during photocatalytic inactivation under VL irradiation.

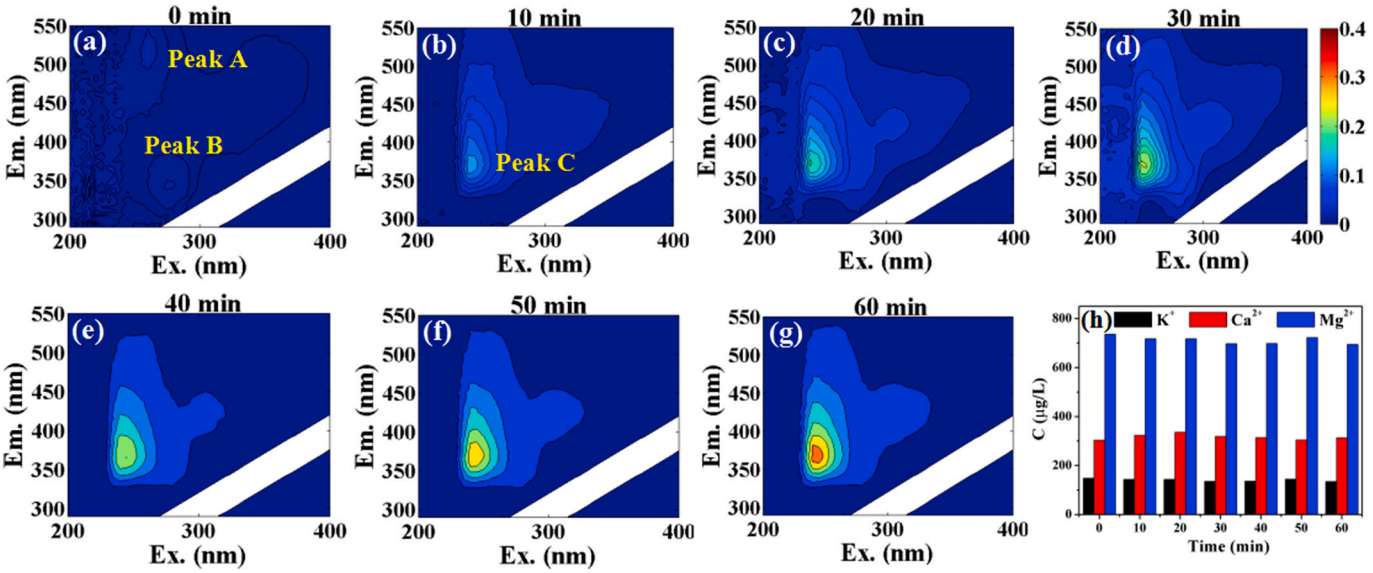

Fig. 7. (a–g) Fluorescence excitation–emission matrix (EEM) spectroscopy of released organic matter from *K. mikimotoi* cell solutions during photocatalytic inactivation process; (h) Variation of inorganic ions (K^+, Ca^{2+} and Mg^{2+}) during photocatalytic inactivation process of algae.

Giaquinto, 2020). In addition, the inorganic matter variation was also monitored during the photocatalytic process (Fig. 7(h)). It was found that the concentration of major inorganic ions K^+, Ca^{2+}, and Mg^{2+} remained unchanged, indicating *K. mikimotoi* inactivation by the present photocatalytic method posed minimal impacts on the seawater environments.

Previous studies have shown that *K. mikimotoi* can secrete haemolytic and cytotoxic substance. To evaluate the toxicity and potential risks to the marine ecosystems during photocatalytic treatment, the evolution of acute toxicity of the algal suspension and released substance was studied using luminescent bacteria (*V. fischeri*) as the subject organism. It was found that the inhibition ratio of bioluminescence for the algal suspension significantly decreased from 46.34% to 7.17% after 60 min of treatment. In contrast, the inhibition ratio of bioluminescence for the released substance (filtered solution) remained the same at a low level of ~7.2% (Fig. 8). This suggests that at the initial stage, the toxicity of the *K. mikimotoi* cells was high which caused the high inactivation of luminescent bacteria, while the released substance had low cytotoxicity, indicating the toxic effect of *K. mikimotoi* was contact-dependent and mainly existed on the *K. mikimotoi* cell membrane. With photocatalytic treatment, the toxicity of the algal suspension was deceased due to the rapture of cells. This also confirmed that toxicity of *K. mikimotoi* was derived from the intact algal cell rather than the released toxins. The present photocatalytic treatment was able to not only inactivate but also lyse the *K. mikimotoi* cells to destroy the cell membrane, so that complete detoxification could be reached.

On the basis of above results, the inactivation mechanism for *K. mikimotoi* was illustrated in Fig. 9. With VL irradiation, the photocatalytic system generated ROSs, in which photo-generated h^+ and $^1O_2$ were found to be the dominant active species to attack the algal cells, resulting in severe oxidative damage to the cell envelope and leading to the destroy of antioxidant enzyme system and departure of nucleus. Overall, the *K. mikimotoi* cells were inactivated and lysed, which significantly decreased the cytotoxicity, and the leakage of intracellular components posed minimal impacts on marine ecosystems after the photocatalytic treatment.

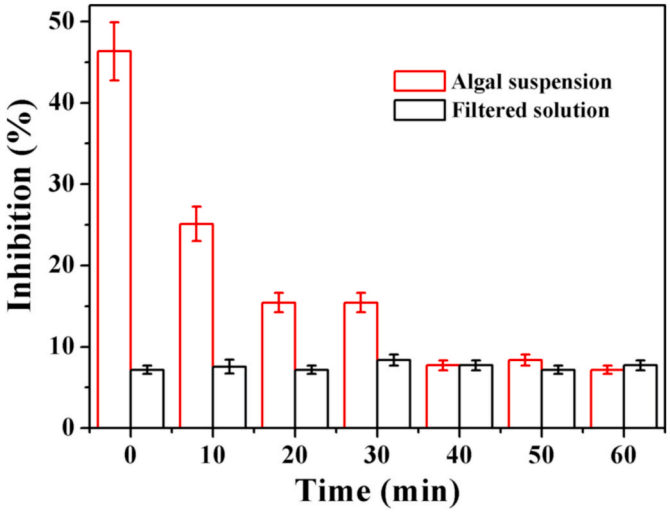

Fig. 8. Evolution of acute toxicity of both algal suspension and filtered solution evaluated by inhibition efficiency towards *V. fischeri* during photocatalytic inactivation process of *K. mikimotoi*.

4. Conclusions

In summary, the photocatalytic inactivation mechanism against

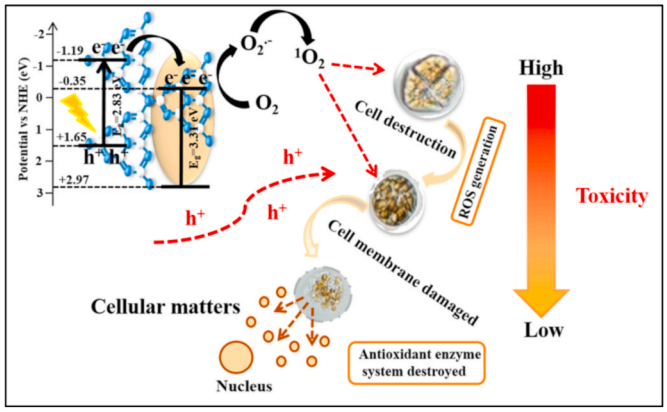

Fig. 9. Schematic illustration of overall photocatalytic inactivation mechanisms of *K. mikimotoi* over g-C_3N_4/TiO_2 film photocatalyst under VL irradiation ($\lambda \geq 420$ nm).

marine harmful microalgae *K. mikimotoi* was investigated for the first time. TiO_2/g-C_3N_4 immobilized films were utilized as model photocatalysts under VL irradiation, which could achieve 64% inactivation efficiency within 60 min, evaluated by monitoring the *in vivo* chlorophyll-a fluorescence. This immobilized photocatalytic film possessed high photo-stability, and was able to be easily recycled for four times with negligible activity loss. Roles of photo-generated h^+ and $^1O_2$ as the major reactive species were confirmed by scavenging study combined with quantitatively analysis of specific ROSs. The cell membrane was found to be the first attacking sites which caused lipid peroxidation and increase of membrane permeability, followed by induction of antioxidant enzyme system (i.e. up-regulation of CAT and SOD) to quench intracellular ROSs. The complete lysis of cell structure was observed with departure of nucleus. In addition, intracellular release profile and acute toxicity assessment indicated the toxicity of *K. mikimotoi* was contact-dependent, which can be detoxified by lysing of the cells during photocatalytic treatment. Due to the merits of direct utilizing solar energy, the present treatment methodology shows potential to be a promising and sustainable alternative to *in-situ* controlling harmful microalgae at sea environments in the future.

Declaration of competing interest

The authors declare that they have no known competing financial interests or personal relationships that could have appeared to influence the work reported in this paper.

Acknowledgements

Special appreciation is expressed to the Culture Collection of Marine Microalgae of Jinan University for provision and cultivation of *Karenia mikimotoi* strain. This work was supported by Science and Technology Program of Guangzhou, China (202002030177), Guangdong Basic and Applied Basic Research Foundation for Distinguished Young Scholars (2021B1515020063), National Natural Science Foundation of China (21607028, U1901210 and 41606175), National Key Research and Development Program of China (2019YFC1804501), and Local Innovative and Research Teams Project of Guangdong Pearl River Talents Program (2017BT01Z032).

Appendix A. Supplementary data

Supplementary data to this article can be found online at https://doi.org/10.1016/j.envres.2021.111295.

Credit statement

Wanjun Wang: Formal analysis, Methodology, Writing – original draft. Pan Liao: Formal analysis, Methodology. Guiying Li: Investigation. Heng Chen: Investigation. Jingyi Cen: Methodology. Songhui Lu: Data curation. Po Keung Wong: Validation. Taicheng An: Conceptualization, Supervision.

References

Anderson, D.M., Cembella, A.D., Hallegraeff, G.M., 2012. Progress in understanding harmful algal blooms: paradigm shifts and new technologies for research, monitoring, and management. Ann. Rev. Mar. Sci. 4, 143–176.

Atinafu, D.G., Yun, B.Y., Wi, S., Kang, Y., Kim, S., 2021. A comparative analysis of biochar, activated carbon, expanded graphite, and multi-walled carbon nanotubes with respect to PCM loading and energy-storage capacities. Environ. Res. 195, 110853.

Berdalet, E., Fleming, L.E., Gowen, R., Davidson, K., Hess, P., Backer, L.C., Moore, S.K., Hoagland, P., Enevoldsen, H., 2015. Marine harmful algal blooms, human health and wellbeing: challenges and opportunities in the 21st century. J. Mar. Biol. Assoc. U. K. 96 (1), 61–91.

Beutler, M., Wiltshire, K.H., Meyer, B., Moldaenke, C., Luring, C., Meyerhofer, M., Hansen, U.P., Dau, H., 2002. A fluorometric method for the differentiation of algal populations *in vivo* and *in situ*. Photosynth. Res. 72 (1), 39–53.

Bhuvaneshwari, M., Thiagarajan, V., Nemade, P., Chandrasekaran, N., Mukherjee, A., 2018. Toxicity and trophic transfer of P25 TiO_2 NPs from *Dunaliella salina* to *Artemia salina*: effect of dietary and waterborne exposure. Environ. Res. 160, 39–46.

Boonprakob, N., Wetchakun, N., Phanichphant, S., Waxler, D., Sherrell, P., Nattestad, A., Chen, J., Inceesungvorn, B., 2014. Enhanced visible-light photocatalytic activity of g-C_3N_4/TiO_2 films. J. Colloid Interface Sci. 417, 402–409.

Carpentier, C., Dahlhaus, A., van de Giesen, N., Marsalek, B., 2013. The influence of hard substratum reflection and calibration profiles on in situ fluorescence measurements of benthic microalgal biomass. Environ. Sci. Process. Impacts 15 (4), 783–793.

Chang, F.H., 2011. Toxic effects of three closely-related dinoflagellates, *Karenia concordia, K. brevisulcata* and *K. mikimotoi* (Gymnodiniales, Dinophyceae) on other microalgal species. Harmful Algae 10 (2), 181–187.

Chang, F.H., Gall, M., 2013. Pigment compositions and toxic effects of three harmful Karenia species, *Karenia concordia, Karenia brevisulcata* and *Karenia mikimotoi* (Gymnodiniales, Dinophyceae), on rotifers and brine shrimps. Harmful Algae 27, 113–120.

Chen, J.S., Lou, X.W., 2010. The superior lithium storage capabilities of ultra-fine rutile TiO_2 nanoparticles. J. Power Sources 195 (9), 2905–2908.

Eugene, A.J., Guzman, M.I., 2019. Production of singlet oxygen $^1O_2$ during the photochemistry of aqueous pyruvic acid: the effects of pH and photon flux under steady-state O_2(aq) concentration. Environ. Sci. Technol. 53 (21), 12425–12432.

Fan, G., You, Y., Wang, B., Wu, S., Zhang, Z., Zheng, X., Bao, M., Zhan, J., 2019. Inactivation of harmful cyanobacteria by Ag/AgCl@ZIF-8 coating under visible light: efficiency and its mechanisms. Appl. Catal. B Environ. 256, 117866.

Favero, N.J., Giaquinto, P.C., 2020. Environmental enrichment techniques and tryptophan supplementation used to improve the quality of life and animal welfare of Nile tilapia. Aquacul. Rep. 17, 100354.

Feng, C., Deng, Y., Tang, L., Zeng, G., Wang, J., Yu, J., Liu, Y., Peng, B., Feng, H., Wang, J., 2018. Core-shell Ag_2CrO_4/N-GQDs@g-C_3N_4 composites with anti-photocorrosion performance for enhanced full-spectrum-light photocatalytic activities. Appl. Catal. B Environ. 239, 525–536.

Fu, X., Tang, W., Ji, L., Chen, S., 2012. V_2O_5/Al_2O_3 composite photocatalyst: preparation, characterization, and the role of Al_2O_3. Chem. Eng. J. 180, 170–177.

Glibert, P.M., 2017. Eutrophication, harmful algae and biodiversity-challenging paradigms in a world of complex nutrient changes. Mar. Pollut. Bull. 124 (2), 591–606.

Gobler, C.J., Berry, D.L., Dyhrman, S.T., Wilhelm, S.W., 2011. Niche of harmful alga aureococcus anophagefferens revealed through ecogenomics. Proc. Natl. Acad. Sci. Unit. States Am. 108 (11), 4352–4357.

Guan, W., Li, P., 2017. Dependency of UVR-induced photoinhibition on atomic ratio of N to P in the dinoflagellate Karenia mikimotoi. Mar. Biol. 164 (31), 2–9.

Harris, T.D., Graham, J.L., 2015. Preliminary evaluation of an *in vivo* fluorometer to quantify algal periphyton biomass and community composition. Lake Reservoir Manag. 31 (2), 127–133.

He, Y., Cai, J., Li, T., Wu, Y., Yi, Y., Luo, M., Zhao, L., 2012. Synthesis, characterization, and activity Evaluation of dyVO_4/g-C_3N_4 Composites under visible-light irradiation. Ind. Eng. Chem. Res. 51 (45), 14729–14737.

Jin, Y., Zhang, S., Xu, H., Ma, C., Sun, J., Li, H., Pei, H., 2019. Application of N-TiO_2 for visible-light photocatalytic degradation of *Cylindrospermopsis raciborskii* - more difficult than that for photodegradation of *Microcystis aeruginosa* ? Environ. Pollut. 245, 642–650.

Landsberg, J.H., 2002. The effects of harmful algal blooms on aquatic organisms. Rev. Fish. Sci. 10 (2), 113–390.

Lapointe, B.E., Herren, L.W., Debortoli, D.D., Vogel, M.A., 2015. Evidence of sewage-driven eutrophication and harmful algal blooms in Florida's Indian River Lagoon. Harmful Algae 43, 82–102.

Lei, Q.Y., Lu, S.H., 2011. Molecular ecological responses of the dinoflagellate *Karenia mikimotoi* to phosphate stress. Harmful Algae 12, 39–45.

Li, G., Nie, X., Gao, Y., An, T., 2016. Can environmental pharmaceuticals be photocatalytically degraded and completely mineralized in water using g-C_3N_4/TiO_2 under visible light irradiation?—implications of persistent toxic intermediates. Appl. Catal. B Environ. 180, 726–732.

Li, G.Y., Nie, X., Chen, J.Y., Jiang, Q., An, T.C., Wong, P.K., Zhang, H.M., Zhao, H.J., Yamashita, H., 2015. Enhanced visible-light-driven photocatalytic inactivation of *Escherichia coli* using g-C_3N_4/TiO_2 hybrid photocatalyst synthesized using a hydrothermal-calcination approach. Water Res. 86, 17–24.

Li, L., Shao, C., Lin, T.F., Shen, J., Yu, S., Shang, R., Yin, D., Zhang, K., Gao, N., 2014. Kinetics of cell inactivation, toxin release, and degradation during permanganation of *Microcystis aeruginosa*. Environ. Sci. Technol. 48 (5), 2885–2892.

Li, M., Bao, F., Zhang, Y., Sheng, H., Chen, C., Zhao, J., 2019a. Photochemical aging of soot in the aqueous phase: release of dissolved black carbon and the formation of $^1O_2$. Environ. Sci. Technol. 53 (21), 12311–12319.

Li, X., Yan, T., Yu, R., Zhou, M., 2019b. A review of *karenia mikimotoi*: bloom events, physiology, toxicity and toxic mechanism. Harmful Algae 90, 101702.

Li, X.D., Yan, T., Lin, J.N., Yu, R.C., Zhou, M.J., 2017. Detrimental impacts of the dinoflagellate *Karenia mikimotoi* in Fujian coastal waters on typical marine organisms. Harmful Algae 61, 1–12.

Liu, S., Yu, Z., Song, X., Cao, X., 2018. Physiological and photosynthetic responses of *Karenia mikimotoi* to the modified clay mitigation method. Mar. Pollut. Bull. 133, 491–499.

Liu, Y., Hu, Z., Deng, Y., Tang, Y.Z., 2020. Evidence for production of sexual resting cysts by the toxic dinoflagellate *Karenia mikimotoi* in clonal cultures and marine sediments. J. Phycol. 56 (1), 121–134.

Lu, Z., Zhang, K., Liu, X.L., Shi, Y., 2019. High efficiency inactivation of microalgae in ballast water by a new proposed dual-wave UV-photocatalysis system (UVA/UVC-TiO_2). Environ. Sci. Pollut. Res. 26 (8), 7785–7792.

Ma, Z., Wu, M., Lin, L., Thring, R.W., Yu, H., Zhang, X., Zhao, M., 2017. Allelopathic interactions between the macroalga *Hizikia fusiformis* (Harvey) and the harmful blooms-forming dinoflagellate *Karenia mikimotoi*. Harmful Algae 65, 19–26.

Moon, G.H., Kim, D.H., Kim, H.I., Bokare, A.D., Choi, W., 2014. Platinum-like behavior of reduced graphene oxide as a cocatalyst on TiO_2 for the efficient photocatalytic oxidation of arsenite. Environ. Sci. Technol. Lett. 1 (2), 185–190.

Mourad, E., Petit, Y.K., Spezia, R., Samojlov, A., Summa, F.F., Prehal, C., Leypold, C., Mahne, N., Slugovc, C., Fontaine, O., Brutti, S., Freunberger, S.A., 2019. Singlet oxygen from cation driven superoxide disproportionation and consequences for aprotic metal–O_2 batteries. Energy Environ. Sci. 12 (8), 2559–2568.

Murphy, K., Ruiz, G., Dunsmuir, W.M., Davidwaite, T., 2006. Optimized parameters for fluorescence-based verification of ballast water exchange by ships. Environ. Sci. Technol. 40, 2357–2362.

Murphy, K.R., Hambly, A., Singh, S., Henderson, R.K., Baker, A., Stuetz, R., Khan, S.J., 2011. Organic matter fluorescence in municipal water recycling schemes: toward a unified PARAFAC model. Environ. Sci. Technol. 45 (7), 2909–2916.

Natarajan, S., Lakshmi, D.S., Thiagarajan, V., Mrudula, P., Chandrasekaran, N., Mukherjee, A., 2018. Antifouling and anti-algal effects of chitosan nanocomposite (TiO_2/Ag) and pristine (TiO_2 and Ag) films on marine microalgae *Dunaliella salina*. J. Environ. Chem. Eng. 6 (6), 6870–6880.

Ou, H., Gao, N., Deng, Y., Qiao, J., Zhang, K., Li, T., Dong, L., 2011. Mechanistic studies of *Microcystic aeruginosa* inactivation and degradation by UV-C irradiation and chlorination with poly-synchronous analyses. Desalination 272 (1–3), 107–119.

Paerl, H.W., Scott, J.T., McCarthy, M.J., Newell, S.E., Gardner, W.S., Havens, K.E., Hoffman, D.K., Wilhelm, S.W., Wurtsbaugh, W.A., 2016. It takes two to tango: when and where dual nutrient (N & P) reductions are needed to protect lakes and downstream ecosystems. Environ. Sci. Technol. 50 (20), 10805–10813.

Qi, J., Lan, H., Liu, R., Liu, H., Qu, J., 2020. Efficient *Microcystis aeruginosa* removal by moderate photocatalysis-enhanced coagulation with magnetic Zn-doped Fe_3O_4 particles. Water Res. 171, 115448.

Ren, Y., Xu, N., Duan, S., 2006. The study of using TD-700 fluorometer to determine the biomass of microalgal. Ecol. Sci. 25 (2), 128–130.

Rodriguez-Gonzalez, V., Obregon-Alfaro, S., Torres-Martinez, L.M., Cho, S.H., Lee, S.W., 2010. Silver-TiO_2 nanocomposites: synthesis and harmful algae bloom UV-photoelimination. Appl. Catal. B Environ. 98 (3–4), 229–234.

Ruban, A.V., Johnson, M.P., Duffy, C.D., 2012. The photoprotective molecular switch in the photosystem II antenna. Biochim. Biophys. Acta 1817 (1), 167–181.

Serra, A., Pip, P., Gomez, E., Philippe, L., 2020. Efficient magnetic hybrid ZnO-based photocatalysts for visible-light-driven removal of toxic cyanobacteria blooms and cyanotoxins. Appl. Catal. B Environ. 268, 118745.

She, X., Xu, H., Xu, Y., Yan, J., Xia, J., Xu, L., Song, Y., Jiang, Y., Zhang, Q., Li, H., 2014. Exfoliated graphene-like carbon nitride in organic solvents: enhanced photocatalytic activity and highly selective and sensitive sensor for the detection of trace amounts of Cu^{2+}. J. Mater. Chem. 2 (8), 2563.

Song, J., Wang, X., Ma, J., Wang, X., Wang, J., Zhao, J., 2018. Visible-light-driven in situ inactivation of *Microcystis aeruginosa* with the use of floating g-C_3N_4 heterojunction photocatalyst: performance, mechanisms and implications. Appl. Catal. B Environ. 226, 83–92.

Song, J., Wu, X., Zhang, M., Liu, C., Yu, J., Sun, G., Si, Y., Ding, B., 2020. Highly flexible, core-shell heterostructured, and visible-light-driven titania-based nanofibrous membranes for antibiotic removal and E. coil inactivation. Chem. Eng. J. 379, 122269.

Tawakoli, P.N., Al-Ahmad, A., Hoth-Hannig, W., Hannig, M., Hannig, C., 2013. Comparison of different live/dead stainings for detection and quantification of adherent microorganisms in the initial oral biofilm. Clin. Oral Invest. 17 (3), 841–850.

Tian, J., Wu, C., Yu, H., Gao, S., Li, G., Cui, F., Qu, F., 2018. Applying ultraviolet/persulfate (UV/PS) pre-oxidation for controlling ultrafiltration membrane fouling by natural organic matter (NOM) in surface water. Water Res. 132, 190–199.

Toming, K., Kutser, T., Laas, A., Sepp, M., Paavel, B., Nõges, T., 2016. First experiences in mapping lake water quality parameters with sentinel-2 MSI imagery. Rem. Sens. 8 (8), 640.

Tong, Z., Yang, D., Xiao, T., Tian, Y., Jiang, Z., 2015. Biomimetic fabrication of g-C_3N_4/TiO_2 nanosheets with enhanced photocatalytic activity toward organic pollutant degradation. Chem. Eng. J. 260, 117–125.

Wang, D., Zhao, L., Ma, H., Zhang, H., Guo, L.H., 2017. Quantitative analysis of reactive oxygen species photogenerated on metal oxide nanoparticles and their bacteria toxicity: the role of superoxide radicals. Environ. Sci. Technol. 51 (17), 10137–10145.

Wang, W., Wang, H., Li, G., An, T., Zhao, H., Wong, P.K., 2019. Catalyst-free activation of persulfate by visible light for water disinfection: efficiency and mechanisms. Water Res. 157, 106–118.

Wang, W., Yu, Y., An, T., Li, G., Yip, H.Y., Yu, J.C., Wong, P.K., 2012. Visible-light-driven photocatalytic inactivation of E. coli K-12 by bismuth vanadate nanotubes: bactericidal performance and mechanism. Environ. Sci. Technol. 46 (8), 4599–4606.

Xia, B., Chen, B., Sun, X., Qu, K., Ma, F., Du, M., 2015a. Interaction of TiO_2 nanoparticles with the marine microalga *Nitzschia closterium*: growth inhibition, oxidative stress and internalization. Sci. Total Environ. 508, 525–533.

Xia, D., Shen, Z., Huang, G., Wang, W., Yu, J.C., Wong, P.K., 2015b. Red phosphorus: an earth-abundant elemental photocatalyst for "green" bacterial inactivation under visible light. Environ. Sci. Technol. 49 (10), 6264–6273.

Xu, H., Pei, H., Xiao, H., Li, X., Ma, C., Hu, W., 2016. Inactivation of *Microcystis aeruginosa* by hydrogen-terminated porous Si wafer: performance and mechanisms. J. Photochem. Photobiol., B 158, 23–29.

Yang, Z.B., Takayama, H., Matsuoka, K., Hodgkiss, I.J., 2019. *Karenia digitata sp. nov.* (Gymnodiniales, Dinophyceae), a new harmful algal bloom species from the coastal waters of west Japan and Hong Kong. Phycologia 39 (6), 463–470.

You, Y., Nam, W., 2014. Designing photoluminescent molecular probes for singlet oxygen, hydroxyl radical, and iron–oxygen species. Chem. Sci. 5 (11), 4123–4135.

Zhang, C., Yi, Y.L., Hao, K., Liu, G.L., Wang, G.X., 2013. Algicidal activity of *Salvia miltiorrhiza* bung on *Microcystis aeruginosa*-towards identification of algicidal substance and determination of inhibition mechanism. Chemosphere 93 (6), 997–1004.

Zhang, X., Li, B., Xu, H., Wells, M., Tefsen, B., Qin, B., 2019. Effect of micronutrients on algae in different regions of Taihu, a large, spatially diverse, hypereutrophic lake. Water Res. 151, 500–514.